

Wave Effects in Double-Plane Lensing

RAHUL RAMESH¹, ASHISH KUMAR MEENA^{1,2} and JASJEET SINGH BAGLA^{1*}

¹Department of Physical Sciences, IISER Mohali, Sector 81, SAS Nagar, Punjab, India - 140306.

²Physics Department, Ben-Gurion University of the Negev, P.O. Box 653, Be'er-Sheva 8410501, Israel

*Corresponding author. E-mail: jasjeet@iisermohali.ac.in

MS received xx yy 2021; accepted xx yy 2021

Abstract. We discuss the wave optical effects in gravitational lens systems with two point mass lenses in two different lens planes. We identify and vary parameters (i.e., lens masses, related distances, and their alignments) related to the lens system to investigate their effects on the amplification factor. We find that due to a large number of parameters, it is not possible to make generalized statements regarding the amplification factor. We conclude by noting that the best approach to study two-plane and multi-plane lensing is to study various possible lens systems case by case in order to explore the possibilities in the parameter space instead of hoping to generalize the results of a few test cases. We present a preliminary analysis of the parameter space for a two-lens system here.

Keywords. gravitational waves—microlensing—multi-plane lensing.

1. Introduction

In the last few decades, gravitational lensing has become a useful tool to probe properties of the Universe (Bartelmann, 2010; Kneib & Natarajan, 2011; Umetsu, 2020). However, most of its applications are discussed in the context of gravitational lensing of Electromagnetic (EM) radiation originating from a distant source. Recent detection of gravitational wave (GW) signals from merging compact objects by Laser Interferometer Gravitational-Wave Observatory (LIGO; Abbott *et al.*, 2019, 2020) has opened a new avenue for application of gravitational lensing.

GWs are subject to deflection due to intervening matter as they travel from the source to the observer (Ohanian, 1974; Baraldo *et al.*, 1999) in a manner similar to EM waves. As the GW signal in these direct observations originates from sources at cosmological distances, the possibility of strong lensing due to an intervening galaxy or galaxy cluster is significant (Li *et al.*, 2018; Smith *et al.*, 2018; Broadhurst *et al.*, 2019, 2018, 2020). For gravitational lensing of GW signals in the LIGO frequency range, lensing due to a galaxy or a galaxy cluster can be described in the same manner as that of EM radiation, i.e., in the geometric optics limit. This is possible as the Schwarzschild radius of the lens is much larger in comparison to the wavelength of the GW signal ($R_{\text{Sch}} \gg \lambda_{\text{GW}}$). However, the same is not true for gravitational lensing of GWs (in LIGO frequency range) due to stellar mass

objects, as the wavelength of GW signal in this case is comparable to the Schwarzschild radius of the lens ($R_{\text{Sch}} \sim \lambda_{\text{GW}}$). As a result, wave effects becomes significant, and this leads to frequency dependent amplification of GWs. These wave effects due to an isolated single/double point mass lens (e.g., Takahashi & Nakamura, 2003; Christian *et al.*, 2018) or a point mass with external effects (e.g., Diego *et al.*, 2019; Meena & Bagla, 2020; Mishra *et al.*, 2021) have been discussed in recent studies and it has been shown that if the point mass lens is embedded in an external environment then the wave effects may obtain a significant boost.

In the above studies, only a single lens plane was considered. Another interesting scenario is the lensing due to a double plane lens. Subramanian & Chitre (1984) were amongst the first to explore the framework of double plane lensing due to galaxy scale lenses, and Subramanian *et al.* (1987) applied the formalism to consider dual dark matter halos as double plane lenses. Kochanek & Apostolakis (1988) later pointed out that the population of double plane lenses is small, and is only expected to be approximately 1% – 10% of all lensed systems. Although the gravitational lensing of gravitational waves due to galaxy scale lenses in double plane configuration can be studied using the conventional geometric approach, the microlenses residing in these lens galaxies can lead to wave effects. As these microlenses are lying in two different lens planes, the corresponding wave effects can be significantly different from the case of one or two-point mass lenses in sin-

gle plane. Erdl & Schneider (1993) presented a detailed study of two-point mass lens in double plane lensing in the geometric optics limit and pointed out various differences between single and double-plane lensing.

In the present work, we focus on the wave effects in double plane lensing due to two point mass lenses. While we consider both the point lenses as isolated lenses for the bulk of the paper, we also briefly explore cases wherein these lenses are embedded in foreign galaxies. The method to calculate the amplification factor in a generalized N-plane lensing scenario is presented in Yamamoto (2003). For reference, we also briefly explore the one and two-point mass single plane lenses. To the best of our knowledge, the dependence of the amplification factor of the two-point mass single (or double) plane lens on its various parameters has not been studied in as much detail as what we present.

The rest of the paper is organised as follows: In §2., we review the basics of geometric and wave optics in gravitational lensing. In §3., we revisit the single and double point mass lens in a single plane. In §4., we explore the double plane lensing due to two point masses in detail: this is the core part of our work. Summary and conclusions are presented in §5..

2. Gravitational Lensing

In this section, we briefly review the relevant basics of gravitational lensing in the geometric optics regime (Schneider *et al.*, 1992) and wave optics regime (Takahashi & Nakamura, 2003) for a single lens plane. The gravitational lensing of a distant source by an intermediate lens mass distribution (between source and observer) can be described by the so-called gravitational lens equation,

$$\mathbf{y} = \mathbf{x} - \boldsymbol{\alpha}(\mathbf{x}), \quad (1)$$

where $\mathbf{x} = \boldsymbol{\xi}/\xi_0$, $\mathbf{y} = \boldsymbol{\eta}D_d/\xi_0D_s$ are the dimensionless source and image positions in the source and lens plane, respectively, and ξ_0 is an arbitrary length scale. D_d , D_s and D_{ds} are the angular diameter distances from observer to lens, observer to source and from lens to source, respectively. $\boldsymbol{\alpha}(\mathbf{x})$ is the scaled deflection angle and related to the lens potential as: $\boldsymbol{\alpha}(\mathbf{x}) = \nabla\psi(\mathbf{x})$. The projected lens potential is given as

$$\psi(\mathbf{x}) = \frac{1}{\pi} \int d^2\mathbf{x}' \kappa(\mathbf{x}') \ln |\mathbf{x} - \mathbf{x}'|, \quad (2)$$

with

$$\kappa(\mathbf{x}) = \frac{\Sigma(\mathbf{x})}{\Sigma_{cr}}, \quad \Sigma_{cr} = \frac{c^2}{4\pi G} \frac{D_s}{D_d D_{ds}}, \quad (3)$$

where κ is known as *convergence* and represents the dimensionless surface mass density of the lens.

For a lensed signal coming from the source, the corresponding time delay (t_d) with respect to the unlensed signal is given by

$$t_d = \frac{\xi_0^2}{c} \frac{D_s}{D_d D_{ds}} (1 + z_d) \left[\frac{(\mathbf{x} - \mathbf{y})^2}{2} - \psi(\mathbf{x}) + \phi_m(\mathbf{y}) \right], \quad (4)$$

where z_d is the lens redshift, ξ_0 is an arbitrary length scale used to make Equation 1 dimensionless and $\phi_m(\mathbf{y})$ is a constant which is independent of lens properties and can be chosen to simplify the calculations.

The above mentioned formalism of gravitational lensing is valid as long as the Schwarzschild radius of the lens is much greater than the wavelength of the signal, i.e., $R_{Sch} \gg \lambda$. Hence, it is applicable in case of gravitational lensing of EM waves originating from a distance source due to a lens in the mass range from stellar mass objects ($\sim 1M_\odot$) to cluster of galaxies ($\sim 10^{15}M_\odot$). On the other hand, if the wavelength of the signal is of the order of the Schwarzschild radius of the lens, then the framework of geometric optics no longer holds and we need to take wave effects into account. For light with wavelength $\sim 1\mu\text{m}$, wave effects are considerable if lens mass is $\sim 10^{-9}M_\odot$.

For gravitational waves in the LIGO frequency range (10 Hz–10⁴ Hz), gravitational lensing due to a galaxy or a cluster of galaxies can be well described using the geometric optics approach outlined above. However, wave effects arise if the signal is lensed by stellar mass objects ($10M_\odot - 10^4M_\odot$; see figure 1 in Meena & Bagla 2020) as the corresponding Schwarzschild radius (R_{Sch}) is of the order of the wavelength of the signal (λ_{GW}).

Thus, in a typical scenario of microlensing of gravitational waves, one cannot use geometric optics as the wave effects are not negligible: these manifest as a frequency dependent amplification factor and phase shift. The corresponding amplification factor which is defined as the ratio of the lensed and unlensed signals is given as (Nakamura & Deguchi, 1999; Takahashi & Nakamura, 2003)

$$F(f, \mathbf{y}) = \frac{D_s \xi_0^2 (1 + z_d)}{c D_d D_{ds}} \frac{f}{i} \int d^2\mathbf{x} \exp[2\pi i f t_d(\mathbf{x}, \mathbf{y})], \quad (5)$$

where f is the frequency of the gravitational wave signal, and the rest of the symbols have their usual meaning. One can see that the amplification factor depends on the frequency of the GW signal. Hence, different frequency components of the signal are modulated by varying factors, unlike the case of achromatic lensing

in the regime of geometric optics. As the amplification factor, $F(f, y)$, is a complex quantity, wave effects modify both the amplitude and the phase of the GW signal.

As we transition towards high frequencies (geometric optics regime), the integral in the above equation turns highly oscillatory and only the stationary points of the time delay (t_d) contribute significantly. The form of Equation 5 in geometric optics is

$$F(f, y) = \sum_i \sqrt{|\mu_j|} \exp(2\pi i f t_{d,j} - i\pi n_j), \quad (6)$$

where $t_{d,j}$ is the value of time delay for j -th image, μ_j is the amplification of the j -th image and n_j is the Morse index with values 0, 1/2, 1 for images corresponding to minima, saddle and maxima of the time delay function, respectively. One can see that phase of the lensed GW signal corresponding to saddle (maxima) gets modified by $e^{-i\pi/2}(e^{-i\pi})$.

3. Single Plane Lensing

3.1 Single Plane One-Point Mass lens

Although one cannot solve Equation 5 analytically for general lens mass models, the isolated point mass lens model has an analytical solution (Peters, 1974):

$$F(\omega, y) = \exp\left[\frac{\pi\omega}{4} + \frac{i\omega}{2} \left\{ \ln\left(\frac{\omega}{2}\right) - 2\phi_m(y) \right\}\right] \Gamma\left(1 - \frac{i\omega}{2}\right) {}_1F_1\left(\frac{i\omega}{2}, 1; \frac{i\omega}{2}y^2\right), \quad (7)$$

where $\omega = 8\pi G(1 + z_d)M_L f/c^3$, $y = |y|$, $\phi_m(y) = (x_m - y)^2/2 - \ln x_m$ with $x_m = (y + \sqrt{y^2 + 4})/2$. Here we have used the Einstein radius of the lens system as the relevant scale length: $\xi_0 = (4GM_L D_d D_{ds}/c^2 D_s)^{1/2}$.

The amplification factor of an isolated point mass lens depends on two parameters: the lens mass M_L , and the source position (y) in the source plane. Figure 1 shows the dependency of $F(f)$ on these two parameters. The top row represents the absolute value of the amplification factor ($|F|$) and the phase shift (θ_F) in left and right panel, respectively, for different source positions (y). Here the lens mass (M_L) has been fixed at $100M_\odot$. Similarly, the bottom row represents the variation in the lens mass M_L with a fixed source position $y = 1$. One can see that for a fixed lens mass, variations in the source position changes the amplitude of the oscillations. As we move the source towards the center, the amplitude of the oscillations increases. However, the frequency of the oscillations decreases. On the other hand, the amplitude of the oscillations is fixed if we fix the source position, and only the rate of oscillations change as we vary the lens mass.

3.2 Single Plane Two-Point Mass lens

In a typical galaxy, approximately half of the stellar mass objects are in binary systems. Hence, a two-point (binary) mass lens is a natural generalization of the isolated point mass lens (Schneider & Weiss, 1986). The lensing potential corresponding to a two-point mass lens is given as

$$\psi(x_1, x_2) = \mu_1 \ln(\mathbf{x} - \mathbf{L}) + \mu_2 \ln(\mathbf{x} + \mathbf{L}), \quad (8)$$

where $(\mu_1, \mu_2) = (M_1/M_T, M_2/M_T)$, with $M_T = M_1 + M_2$. For a two-point mass lens, one can always choose a coordinate system in which both point masses lie on the x -axis and are at equal distance from the center. Hence, the distance vectors for the first and second point masses are $(L, 0)$ and $(-L, 0)$, respectively.

A two-point mass lens system can be described by a total of five parameters, namely, the source position (y_1, y_2), the lens masses (M_1, M_2), and their separation $2L$. Depending on the values of these parameters, one obtains either a three or a five-image configuration. Gravitational lensing due to a binary lens in geometric optics has already been studied in great detail (e.g., Schneider & Weiss, 1986; Witt & Petters, 1993; Asada, 2003; Pejcha & Heyrovský, 2009; Bozza et al., 2020). However, the same is not true for the wave optics regime.

Figure 2 shows the $F(f)$ curves for a binary lens with different values of the above mentioned parameters. The corresponding caustics and critical line plots are shown in Figure 8 in Appendix A.. The top panel in Figure 2 shows the amplitude ($|F|$) and phase shift (θ_F) in the left and right panel, respectively, for different source positions keeping the lens masses and the separation vector fixed. Here, we fix lens masses (M_1, M_2) and the separation vector (\mathbf{L}) to be $(50M_\odot, 50M_\odot)$ and $(0.5, 0)$, respectively. Analogous to a single point mass lens, as we move towards the center, the amplitude of the fluctuations in amplitude and phase shift increases and the frequency of the oscillations decreases. However, the presence of extra images due to the binary lens introduces further fluctuations in the amplitude and phase shift. Instead of the source position, if we vary the mass of the two components of the binary (centre panel), at low frequency ($f < 100\text{Hz}$), we make observations similar to the previous case (and the isolated point mass lens). However, at $f > 100\text{Hz}$, we notice differences due to the varying number of images, the time delay between these images, and the magnification of the various images. This can be seen in the green and blue curves which correspond to $(M_1, M_2) = (50M_\odot, 50M_\odot)$ and $(70M_\odot, 30M_\odot)$. Both these configurations give rise to a five-image geometry (centre panel of Figure 8). However, the blue curve shows significant de-amplification compared to the one in green.

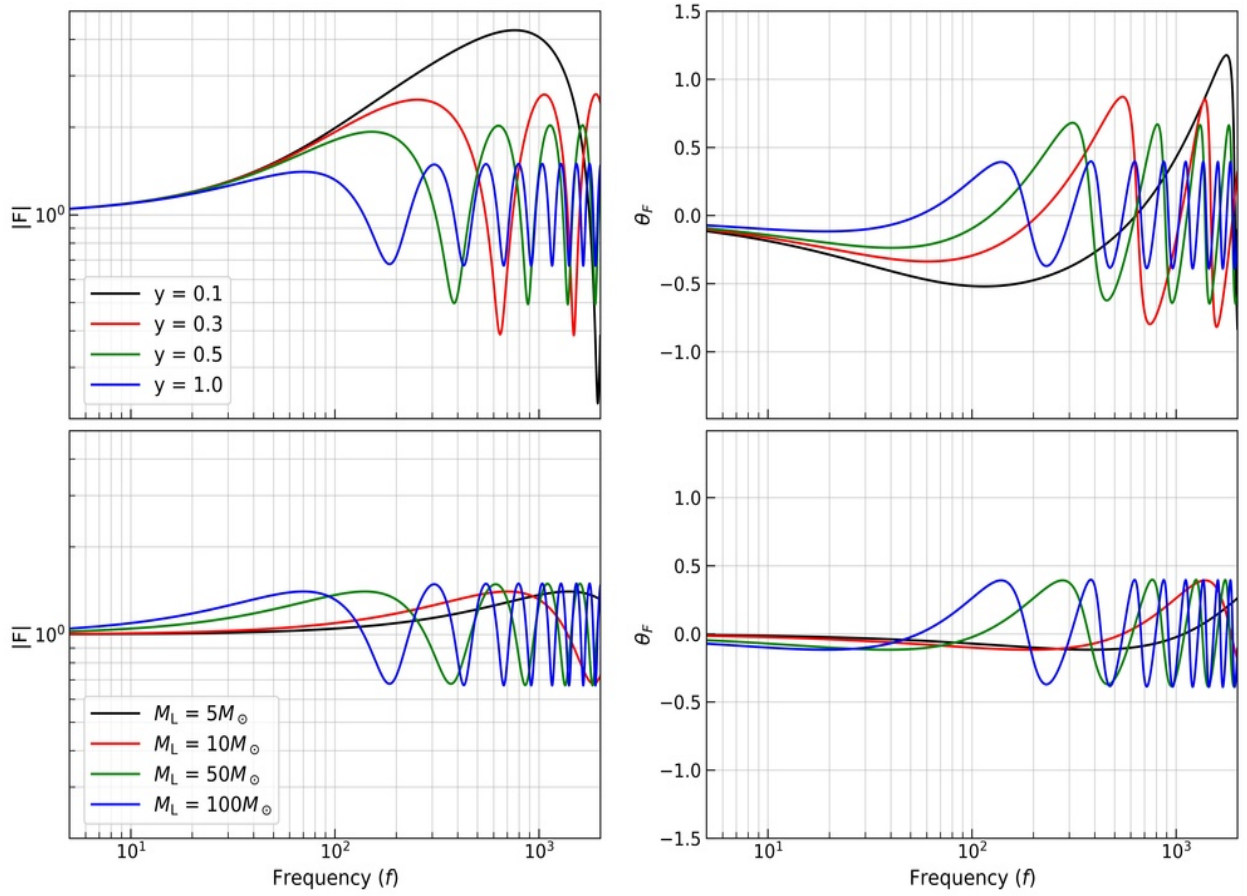


Figure 1. Gravitational lensing due to point mass lens: The top row represents the amplification factor ($|F|$) and phase shift (θ_F) due to a point mass lens of $100M_\odot$ with different source positions (y) in left and right panel, respectively. Similarly, the bottom row shows the amplification factor and phase shift factor due to a point lens with different lens mass values and source position, $y = 1$.

In the bottom panel, we vary the separation between the two lenses by fixing the source position to $(0.1, 0.1)$ and lens masses to $(50M_\odot, 50M_\odot)$. For the case of small values of L , we converge towards the point mass lens as expected ($L = 0.1$; black curve). Increasing the separation leads to different types of interference patterns depending on the number of images and the corresponding time delays.

4. Double-Plane Lensing

The presence of a second lens plane contributes an additional deflection angle in the gravitational lens equation (in thin lens approximation) given as (in dimensionless form; [Schneider et al. 1992](#)),

$$\mathbf{y} = \mathbf{x}_1 - \alpha_1(\mathbf{x}_1) - \alpha_2(\mathbf{x}_2), \quad (1)$$

where \mathbf{y} is the unlensed source position in the source plane. $\alpha_1(\alpha_2)$ is the scaled deflection angle and $\mathbf{x}_1(\mathbf{x}_2)$

is the corresponding impact parameter in the first (second) lens plane, respectively. Due to the additional deflection (introduced by the second lens plane), the gravitational lens equation no longer remains a gradient mapping from image to source plane, leading to new interesting image properties (in geometric optics approximation). The time delay function in case of double-plane lensing is given as

$$t_d(\mathbf{x}_1, \mathbf{x}_2, \mathbf{y}) = t_{12}(\mathbf{x}_1, \mathbf{x}_2) + t_{23}(\mathbf{x}_2, \mathbf{y}), \quad (2)$$

and

$$t_{ij}(\mathbf{x}_i, \mathbf{x}_j) = \frac{1 + z_i}{c} \frac{D_i D_j}{D_{ij}} \left[\frac{(\mathbf{x}_i - \mathbf{x}_j)^2}{2} - \beta_{ij} \psi_1(\mathbf{x}_i) \right], \quad (3)$$

where $\beta_{ij} = D_{ij} D_s / D_j D_{is}$ is a combination of various angular diameter distances related to the lens system with the indices $i, j = 1, 2, 3$, $i < j$ and $j = 3$ represents the source plane. The rest of the symbols have their usual meaning.

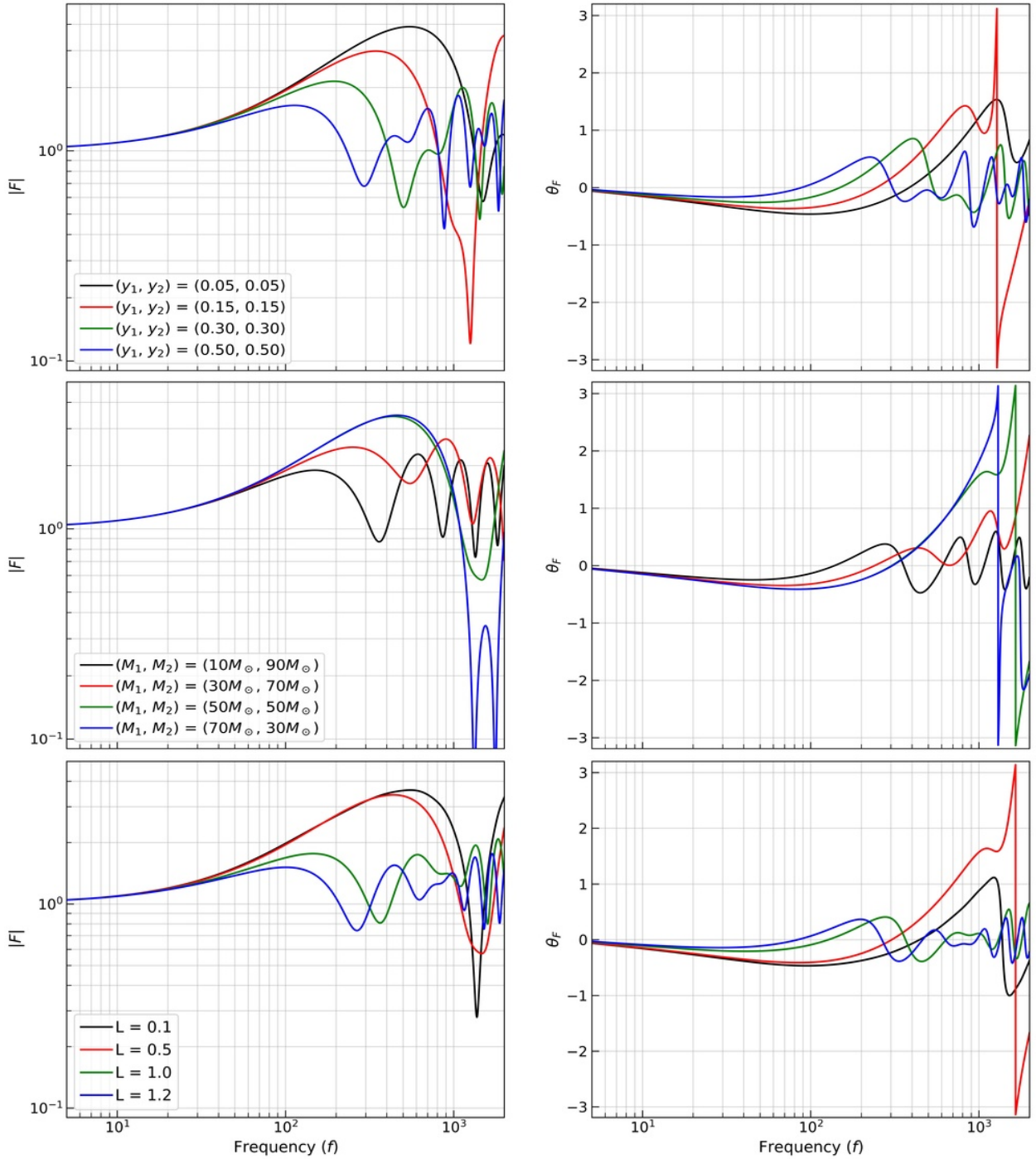


Figure 2. Gravitational lensing due to binary lens: The top row represents the amplification factor ($|F|$) and phase shift (θ_F) due to a binary lens with binary lens masses of $(M_1, M_2) = (50M_\odot, 50M_\odot)$ at a separation (L) = 0.5. The different values of (y_1, y_2) are mentioned in the left panel. The middle row represents the variation in lens masses while fixing the source position to $(y_1, y_2) = (0.1, 0.1)$ and at a separation of (L) = 0.5. The bottom row represents the variation in the separation vector while fixing the source position to $(y_1, y_2) = (0.1, 0.1)$ and binary lens masses $(M_1, M_2) = (50M_\odot, 50M_\odot)$.

Similar to §3., the above mentioned equations are valid only within the regime of geometric optics. To study the wave effects in double plane lensing, one needs to generalize Equation 5. Such a generalization

has been presented in Yamamoto (2003) using path integral formalism developed in Nakamura & Deguchi (1999). In the case of N-plane lens system, the am-

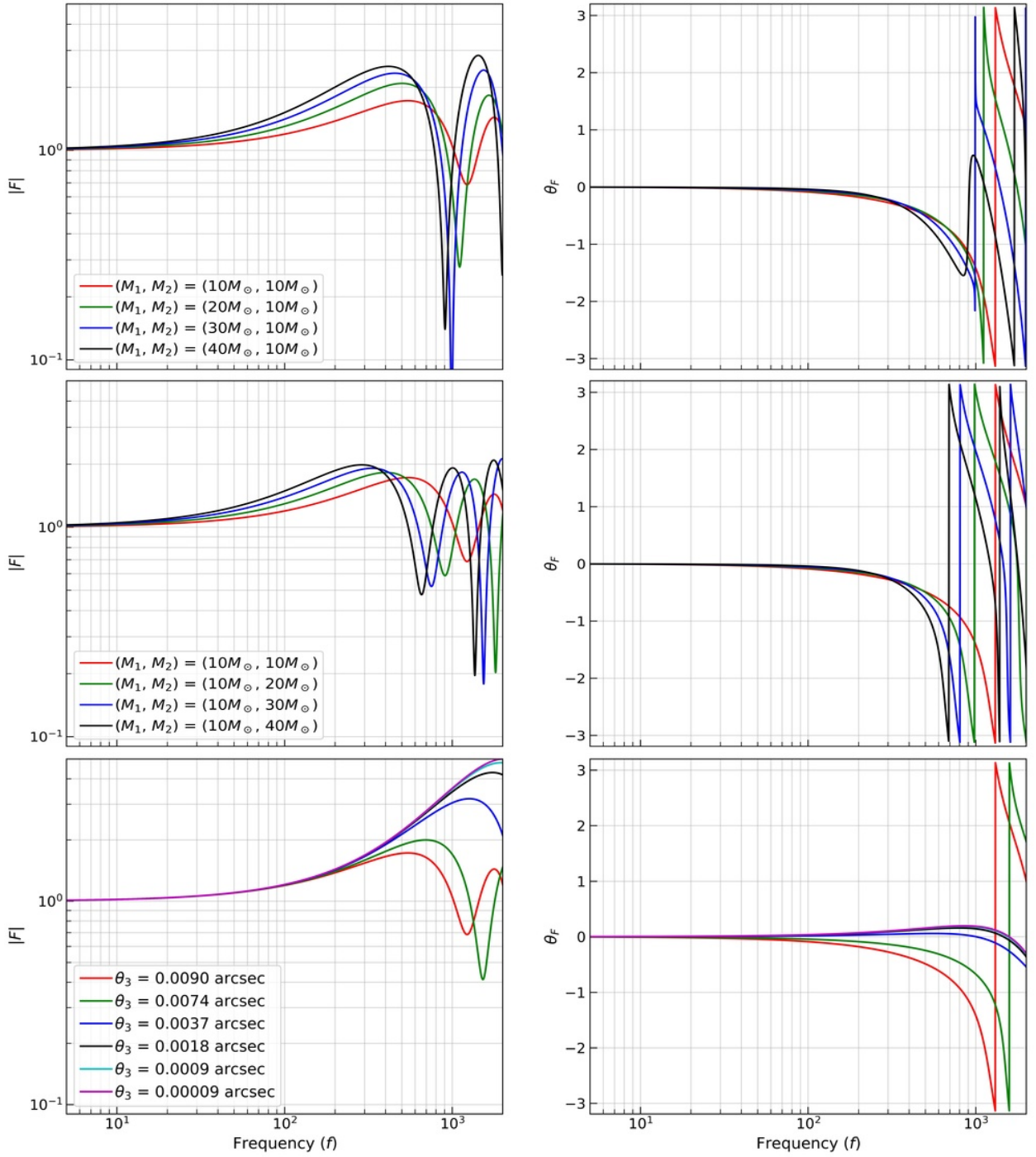


Figure 3. Dependence of the amplification factor (absolute value on the left, and phase ($\Delta\Phi = -i\ln[F/|F|]$) on the right) on various parameters for the special case (Equation 6). We vary one parameter at a time, while keeping the others fixed (with values as explained in detail in the main text). Top panel: As M_1 increases, oscillations become more rapid, and the maximum value of amplification increases as well. Centre panel: Similar to the previous case, oscillations become more rapid, but there is no rise in value of amplification. Also, oscillations here are more rapid in comparison to the previous case. Bottom panel: Angular position of the observer is varied. When the observer is closer to the line joining the source with the two lenses, oscillations are slower, but the amplification is larger. As θ_3 reduces, we also note that the curves tend to converge.

plication factor is given by (Yamamoto, 2003):

(4)

$$F(f, \mathbf{y}) = C f^N \int d^2 \mathbf{x}_1 \dots d^2 \mathbf{x}_N \exp[2\pi i f t_d(\mathbf{x}_1, \dots, \mathbf{x}_N, \mathbf{y})]$$

where different \mathbf{x}_i represent two dimensional vectors

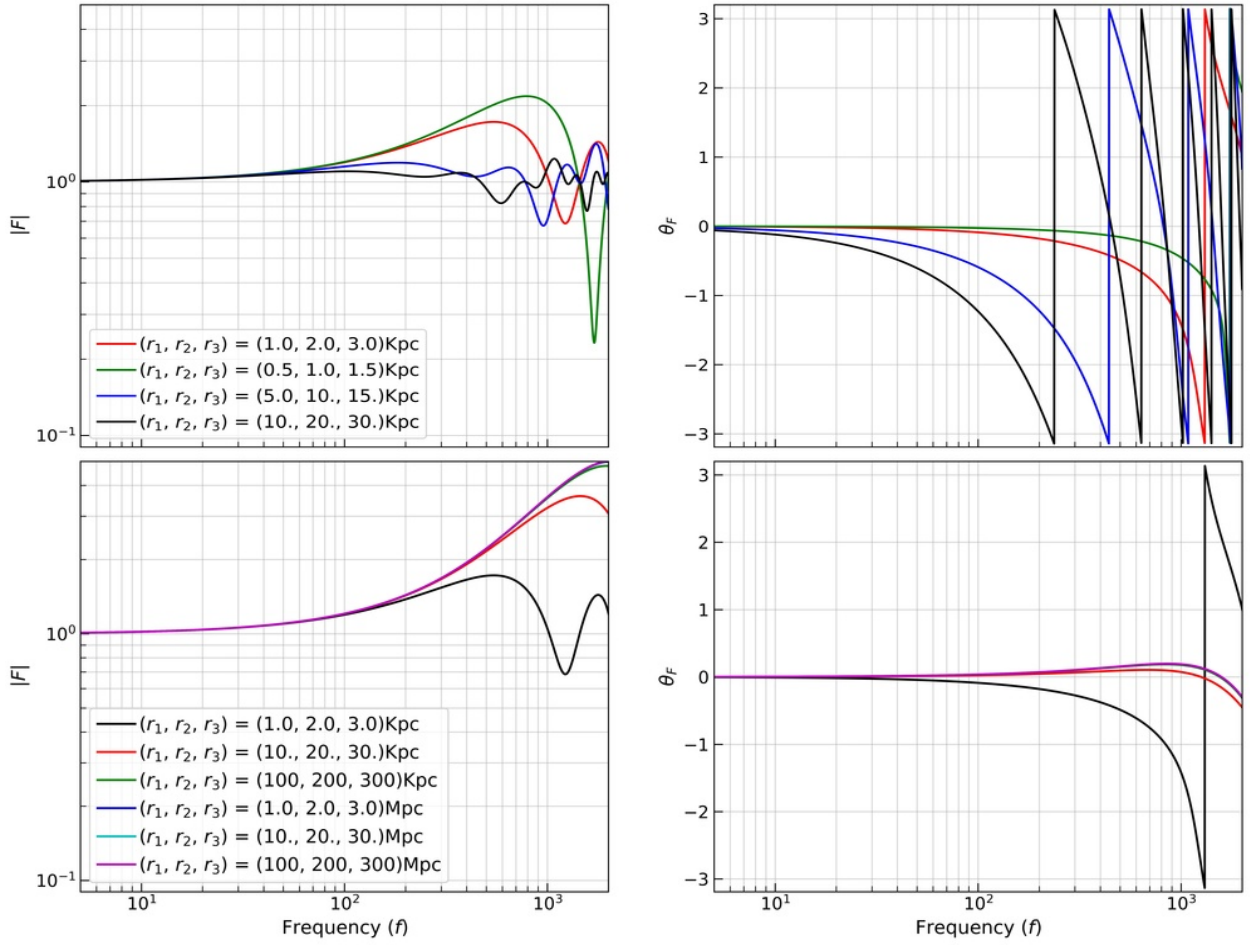


Figure 4. Dependence of the amplification factor on the radial distances of the three objects for the special case (Equation 6). While there are multiple ways to vary the three distances, we do so by maintaining a constant ratio between the three values. In the top panel, we fix the angular position of the observer, while we fix the transverse distance of the observer in the bottom panel. In the former case, we note that greater values of (r_1, r_2, r_3) lead to an increase in rate of oscillation, coupled with a drop in the maximum value of amplification. Trends are opposite in the bottom panel.

in different lens planes. f represents the frequency of the signal. The time delay function is given by $t_d(x_1, \dots, \mathbf{x}_N, \mathbf{y}) = \sum_{i=1}^N t_{i,i+1}(\mathbf{x}_i, \mathbf{x}_{i+1})$ with $\mathbf{x}_{N+1} = \mathbf{y}$. C is a factor which depends on the various angular diameter distances under consideration and given as

$$C = \left(\frac{-i}{c}\right)^N \prod_{i=1}^N (1 + z_i) \frac{D_{0,i} D_{0,i+1}}{D_{i,i+1}}, \quad (5)$$

where z_i is the redshift for the i -th lens plane and $D_{0,i}$, $D_{0,i+1}$, and $D_{i,i+1}$ are the angular diameter distances between observer and i -th lens plane, observer and $(i+1)$ -th lens plane, and i -th and $(i+1)$ -th lens plane.

In general, Equation 4 needs to be solved numerically. However, for a special case of double-plane lensing ($N = 2$), one can obtain an analytic expression (Yamamoto, 2003). This special case is discussed in §4.1. More general cases are discussed in §4.2 and

§4.3. Performing this ‘2N’ integral (Equation 4) using standard quadrature methods is not a very efficient process. Hence, for these general cases, we use a Monte Carlo integrator provided by the VEGAS package (Lepage, 2020).

4.1 The Special Case

Consider two point mass lenses with masses M_1 and M_2 , at distances r_1 and r_2 (from the source) respectively, that are co-linear with the source. For an observer at a distance r_3 and angular position θ_3 , the amplification factor is given by (Yamamoto, 2003):

$$F(k, \theta_3) = \exp(i\alpha) \exp\left(\frac{\pi k G M_T}{c^2}\right) \Gamma(1 - \chi_1) \sum_{L=0}^{\infty} \frac{(-i)^L}{(L!)^2} \Gamma(1 + L - \chi_2) (xz)^L {}_2F_1(1 - \chi_1, 1 + L - \chi_2, 1; 1 - z) \quad (6)$$

where

$$M_T := M_1 + M_2, \quad k := (2\pi f)/c, \quad (7)$$

$$\chi_1 := \frac{2ikGM_1}{c^2}, \quad \chi_2 := \frac{2ikGM_2}{c^2}, \quad (8)$$

$$z := \frac{r_3(r_2 - r_1)}{r_2(r_3 - r_1)}, \quad x := \frac{kr_2r_3\theta_3^2}{2(r_3 - r_2)}, \quad (9)$$

α is a real constant corresponding to a constant phase difference, and ${}_2F_1(a, b, c; d)$ is the Hyper-geometric function.

For the special case under consideration, there are six different parameters on which the amplification factor depends, namely, r_1 , r_2 , r_3 , θ_3 , M_1 and M_2 . In Figure 3, we vary these parameters one at a time. For each case, the absolute value of the amplification factor is shown on the left, while the phase is shown on the right. In the top panel, we fix $(r_1, r_2, r_3) = (1.0, 2.0, 3.0)$ kpc, $M_2 = 10 M_\odot$, $\theta_3 = 0.009$ arc-sec, and vary M_1 . As M_1 increases, oscillations become more rapid, and this is accompanied by an increase in the maximum value of the amplification factor. In the centre panel, we vary the value of M_2 , while keeping $M_1 = 10 M_\odot$ and other parameters fixed at the values mentioned above. As M_2 increases, we again notice that the oscillations become rapid, and the maximum value of the amplification factor also does increase slightly. However, in the case of varying M_2 , oscillations are more rapid than in the case of varying M_1 , and the maximum value of amplification does not change as sharply as in the case of varying M_1 . For instance, the black curve in the centre left panel oscillates with a frequency of ~ 500 Hz, while the frequency of oscillation of the black curve in the top left panel is ~ 700 Hz. This set of observations suggest the following: the mass of the lens closer to the source (M_1) has a greater affect on the maximum value of the modulus of amplification, while M_2 is more important with respect to the rate at which the amplification factor oscillates. We also note the difference in behaviour of the phase at large M_1 .

In the bottom panel, we vary θ_3 while fixing $(r_1, r_2, r_3) = (1.0, 2.0, 3.0)$ kpc, and $(M_1, M_2) = (10, 10)$

M_\odot . As θ_3 decreases, i.e. as the observer approaches the line joining the source with the two lenses, two qualitative trends take place: oscillations become less rapid, and the maximum value of (modulus of) the amplification factor increases. This is qualitatively similar to what one observes in the single lens plane case. We also note that the behaviour of the amplification factor tends to converge as θ_3 reduces (e.g. the cyan and pink curves almost superimpose on one another).

In Figure 4, we vary (r_1, r_2, r_3) while fixing $M_1 = 10 M_\odot$, $M_2 = 10 M_\odot$. In the top panel, we fix the angular position of the source ($\theta_3 = 0.009$ arcsec). While the three distances can be varied in multiple ways, we do so by fixing the ratio between the three values. As the distances get larger, oscillations are more rapid, and the maximum value of amplification is smaller. We note the similarity in observations with those of the bottom panel of Figure 3: increasing θ_3 while keeping the three distances fixed is analogous to keeping θ_3 fixed while increasing the three distances – both lead to an increase in the length of the perpendicular dropped from the observer to the line joining the source with the two lenses.

Instead of fixing the value of θ_3 while varying (r_1, r_2, r_3) , one can alternatively fix the value of the above mentioned perpendicular distance. We show these trends in the bottom panel of Figure 4 where we fix the perpendicular distance to be $\sim 4 \times 10^{12}$ meters. Once again, we note similarities to the bottom panel of Figure 3: as the magnitude of (r_1, r_2, r_3) increases, the angular position of the observer is effectively reduced, and we observe that the oscillations of the amplification factor become less rapid, and the maximum value of (modulus of) the amplification factor increases. Also, the curves tend to converge for large values of the three distances.

4.2 Relaxing the Co-linearity Condition

In this sub-section, we relax the condition that requires the two lenses to be co-linear with the source. Once we relax the same, there are two possible scenarios that one can consider: (1) In-Plane variation of angular positions: the source, lenses and the observer lie along the same plane. This introduces two additional parameters in the analysis, namely, θ_1 and θ_2 – the angular positions of the two lenses with respect to the source. (2) Off-Plane variation of angular positions: the source, lenses and the observer no longer lie along the same plane. In addition to θ_1 and θ_2 , this case has three more parameters, namely, ϕ_1, ϕ_2, ϕ_3 – the angles (measured from the source) subtended by the off-plane object with respect to the plane of the paper.

We start with the In-Plane case, where the two lenses, the source and the observer all lie along the same plane. The corresponding absolute values and

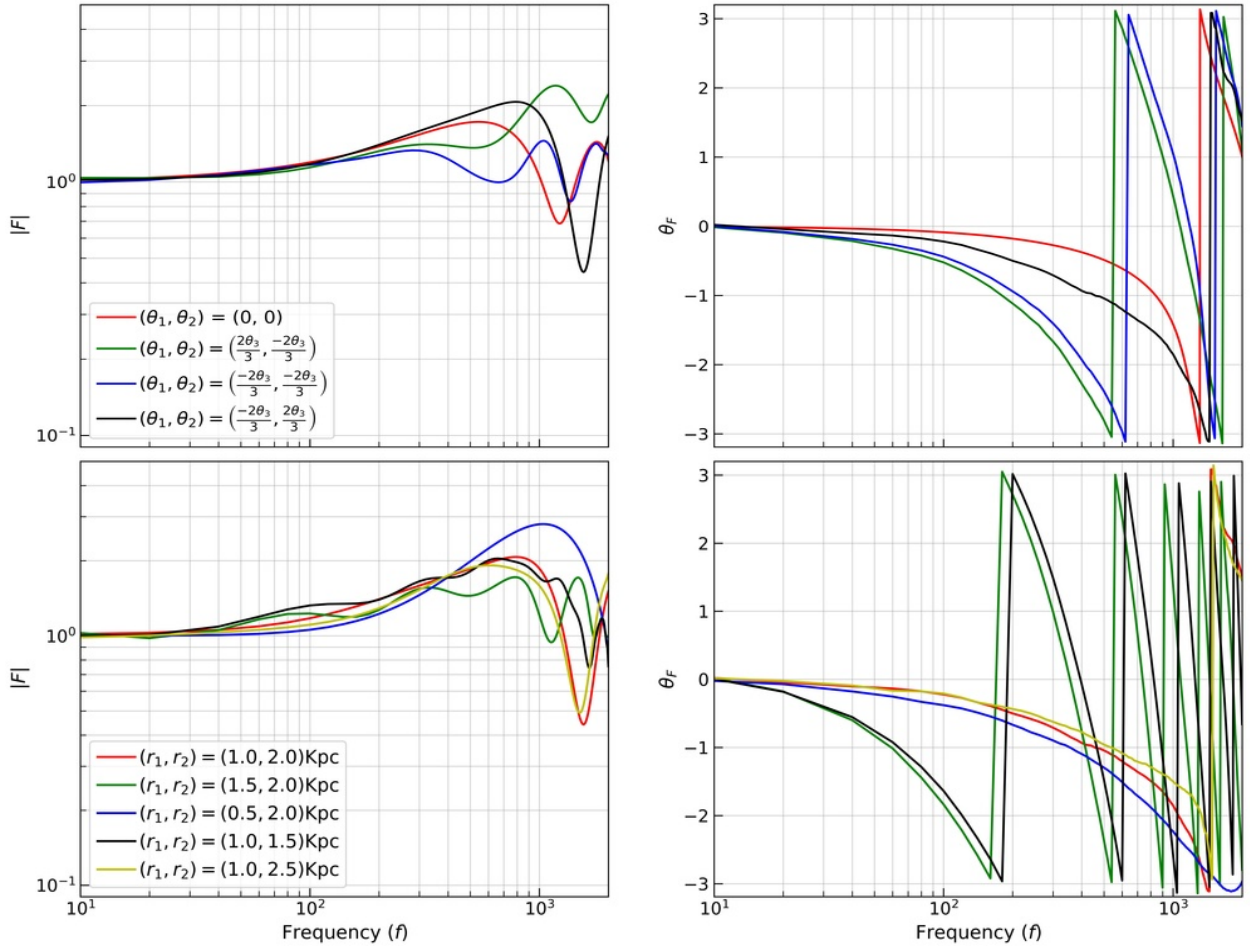


Figure 5. In-Plane Variation of angular positions – Top Panel: Varying the angular position of the two lenses. As elaborated in the main text, the lens closer to the source (M_1) seems to have a greater effect on the range of $|F|$ values, while the rate of oscillation of the $|F|$ curve seems to have a greater dependence on M_2 . Bottom Panel: Varying the radial distance of lenses at fixed values of other parameters. The dependence of the amplification factor on these two parameters seems to be more complex than the dependence on angular positions.

phase of the amplification factors are shown in Figure 5. In the top panel, we choose $(r_1, r_2, r_3) = (1.0, 2.0, 3.0)$ kpc, $(M_1, M_2) = (10, 10) M_\odot$, $\theta_3 = 0.009$ arc-sec, and vary the values of (θ_1, θ_2) . In red, for reference, we consider $(\theta_1, \theta_2) = (0, 0)$, which is the same as some of the curves from Figure 3. For the green and blue curves, we choose $(\theta_1, \theta_2) = (\frac{2\theta_3}{3}, -\frac{2\theta_3}{3})$ and $(-\frac{2\theta_3}{3}, -\frac{2\theta_3}{3})$. These two curves oscillate faster than the curve in red, with the blue curve portraying faster oscillations than the curve in green: oscillations are most rapid when both the lenses are away from the line joining the source with the observer. In the curve in black, we place M_2 closer to the line joining the source with the observer, with $(\theta_1, \theta_2) = (-\frac{2\theta_3}{3}, \frac{2\theta_3}{3})$. In this case, the curve oscillates slower in comparison to the red curve. While the angular positions of both lenses have an impact on both the rate of oscillation and the maximum value of amplification, we note the following difference: the angular

position of M_2 seems to have a greater affect on the rate of oscillation in comparison to the maximum value of amplification. Comparing the blue and green curves, we note the opposite for the angular position of M_1 , which seems to have a greater effect on the maximum value reached by the amplification factor as it oscillates.

In the bottom panel of Figure 5, we continue to choose $(M_1, M_2) = (10, 10) M_\odot$ and $\theta_3 = 0.009$ arc-sec. In addition, we fix $(\theta_1, \theta_2) = (-\frac{2\theta_3}{3}, \frac{2\theta_3}{3})$. For reference, in red, we show the case with $(r_1, r_2) = (1.0, 2.0)$ kpc. With the green and blue (black and yellow) curves, we vary r_1 (r_2) with r_2 (r_1) fixed at 2.0 (1.0) kpc. With the first two set of curves, we see that the rate of oscillation of the amplification factor increases (reduces) as M_1 moves away (closer) to the source. However, with M_2 , we note the opposite: oscillations are more (less) rapid when r_2 is smaller (larger). Unlike in Figure 5, we see that the (radial) position of both the lenses can have

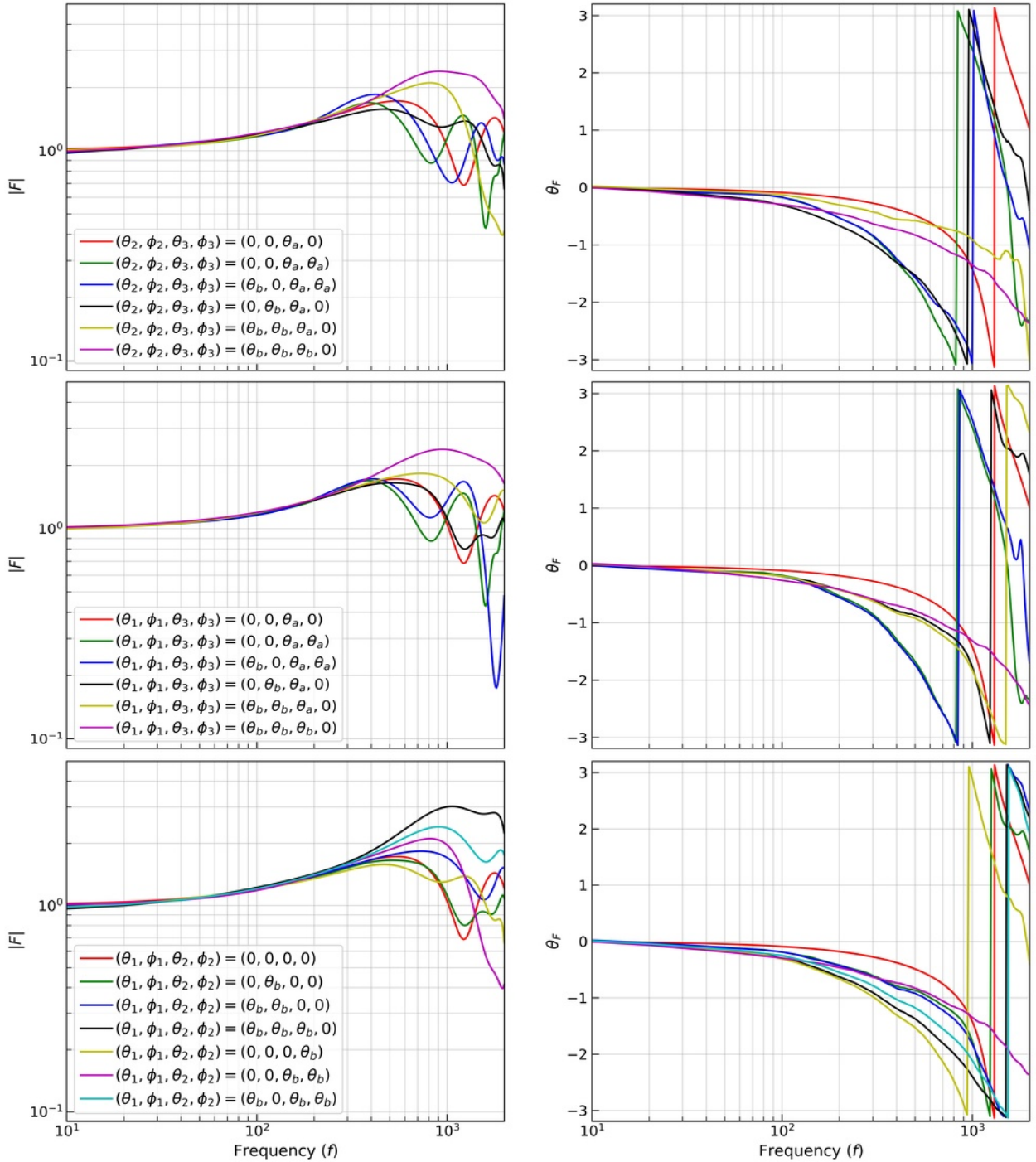


Figure 6. Off-Plane Variation of angular positions – For simplicity, angles are represented by this set of variables: $(\theta_a, \theta_b) = (0.009 \text{ arc-sec}, (2/3)\theta_a)\text{rad}$. As elaborated in the main text, in each panel, we choose one object (along with the source) to form the primary axis of the plane under consideration. One of the other two objects are displaced off-plane. We note that trends are not always similar to in-plane variation of angular positions.

a significant impact on the rate of oscillation. However, only the (radial) position of M_1 greatly effects the maximum value of amplification. This is as opposed to the top panel of Figure 5, where the (angular) position of both the lenses do have an effect on the maximum

value of amplification. We thus already begin to see the complex dependence of the amplification factor on the various parameters, wherein trends are not easy to extrapolate.

Finally, in Figure 6, we show the Off-Plane case.

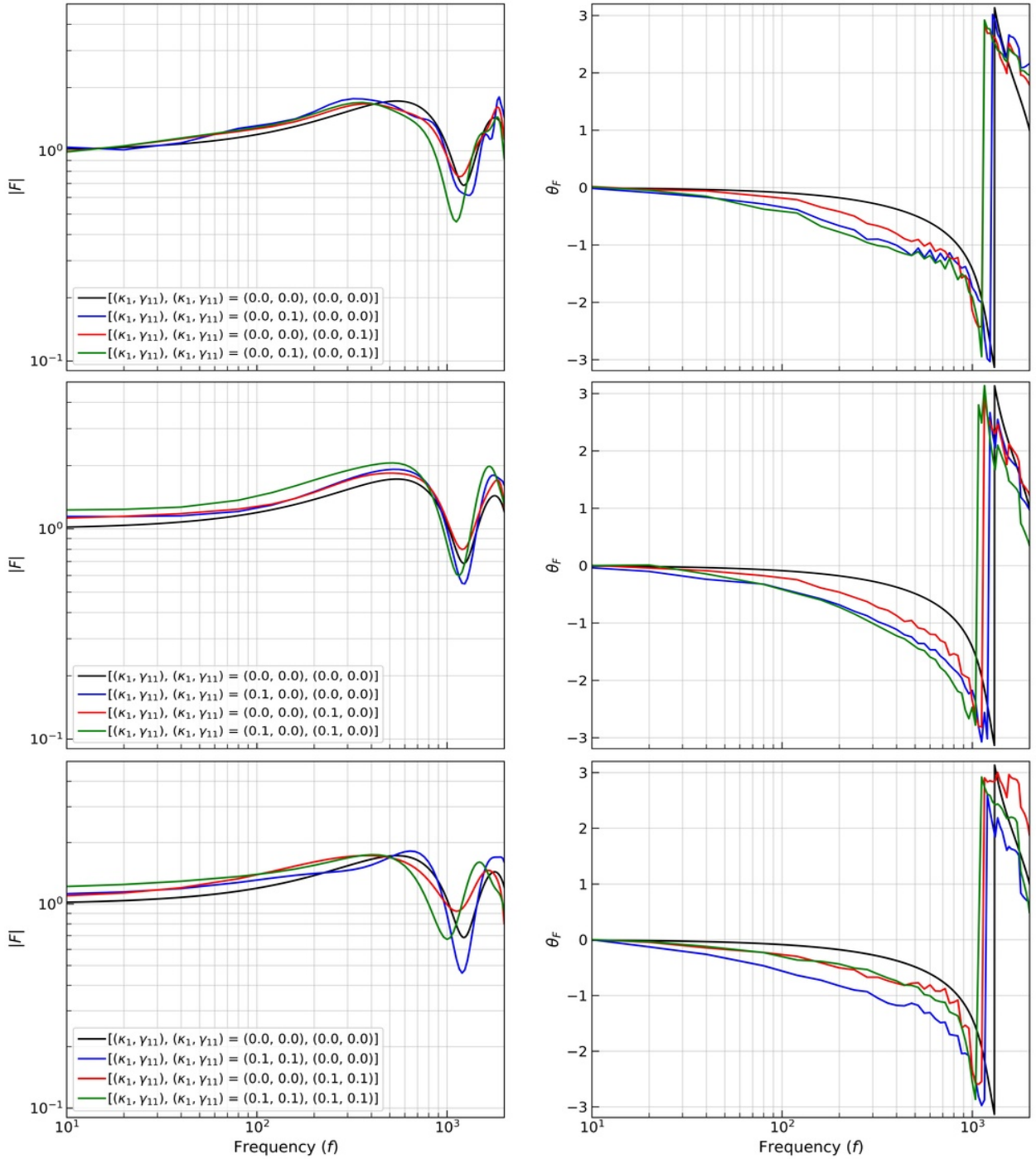


Figure 7. Variation of convergence and shear parameters for the case described in §4.3. In the top (centre) panel, we examine cases with only external shear (convergence). In the bottom panel, we consider non-zero values of both external shear and convergence. External shear seems to have a greater effect on the rate of oscillation, while external convergence modifies the amplification, more so at low frequencies.

As mentioned above, this introduces three additional parameters: ϕ_1, ϕ_2, ϕ_3 , along with the In-Plane parameters, θ_1, θ_2 . Although there are numerous ways in which these parameters can be varied, we choose the following scheme: in each panel, we consider the primary

axis of the plane to be the line joining the source with a given object (lens/observer). The second axis is considered to be the perpendicular dropped from one of the other two objects onto the primary axis. These two axes form the plane, and the third (remaining) object is dis-

placed out of this plane. In all plots, we fix $(r_1, r_2, r_3) = (1.0, 2.0, 3.0)$ kpc, $(M_1, M_2) = (10, 10) M_\odot$. For simplicity, we define $\theta_a = 0.009$ arc-sec and $\theta_b = \frac{2\theta_a}{3}$. Whenever not varied, we fix $(\theta_1, \phi_1) = (\theta_2, \phi_2) = (0, 0)$, and $(\theta_3, \phi_3) = (\theta_a, 0)$ rad.

In the top panel, we consider the line joining the source with M_1 as the primary axis. For reference, in red, we show the case for which the two lenses are collinear with the source. The green and blue curves consider the displacement of the observer from the plane. Both these curves oscillate faster than the reference, with the curve in green oscillating faster than the one in blue. However, the difference in rates of oscillation is not as large as one would expect from a comparison with Figure 5. The remaining three curves consider the displacement of M_2 out of the selected plane. With respect to the reference, the curve in black considers a displacement of M_2 away from the observer. As expected from previous Figures, oscillations grow more rapid, and the modulus curve oscillates to comparatively smaller values. The curve in yellow considers a displacement towards M_2 (albeit an ‘in-plane’ displacement). In this case, we notice that oscillations grow slower and the modulus values oscillate to larger values, both of which are in agreement with earlier observations. In the curve in pink, we reduce the angle of the observer, which essentially brings the observer closer to M_2 . The observed trend is what one would expect from Figure 5: oscillations begin to slow down, and modulus values begin to increase.

In the centre panel, we consider the line joining the source with M_2 as the primary axis. Akin to the previous case, the green and blue curves consider the displacement of the observer from the plane. Observations are qualitatively similar to the previous case: the green and blue curves oscillate faster than the reference, with the green curve oscillating slightly faster. Once again, the difference in rates of oscillation is smaller than expected. In the remaining three curves, M_1 is displaced off-plane. The black curve considers displacement of M_1 away from the observer. As opposed to previous observations, absolute values are similar to the reference, and the rates of oscillation are also comparable. However, if we consider an additional in-plane displacement (yellow curve), the modulus values begin to rise, but not as large as one would expect from Figure 5. Reducing θ_3 (pink curve) seems to increase the modulus values, which is as expected, but the rate of oscillation drops significantly, which contradicts Figure 5. We thus see that a combination of In-Plane and Off-Plane displacements lead to trends that are not always in agreement with In-Plane displacements alone, and the difference is larger for M_1 .

In the bottom panel, we consider the line joining the

source with the observer as the primary axis. Curves two - four (five - seven) consider off-plane displacements of M_1 (M_2). The curve in green considers an off-plane displacement of M_1 away from the observer. From Figure 5, one would expect the curve in green to oscillate faster than the one in red, but such a trend is not seen. However, we note that a slight reduction in the maximum value of amplification, as expected. The curve in blue considers a displacement of M_1 towards the observer, and as expected, this is accompanied by an increase in the maximum value of amplification. The curve in black considers an in-plane displacement of M_2 towards the source, and as expected from previous plots, the rate of oscillation drops. However, we also note a very sharp increase in the maximum value of amplification, which hasn’t always been observed in earlier plots. The curves in yellow and pink consider displacements of M_2 away and towards the observer, respectively. As expected, we note an increase and decrease in the rate of oscillation, respectively. With the curve in cyan, we consider a displacement of M_1 towards the observer, and in agreement with previous plots, we note an increase in the maximum value of amplification.

4.3 Effect of External Perturbations

So far, we have explored cases where both point mass lenses have been treated as isolated objects in their respective lens planes. While this is a starting point for lens systems within our own galaxy, a further generalization is required when lenses are embedded in host galaxies. In this subsection, we consider an extension of the special case discussed in §4.1: scenarios wherein the two micro-lenses are collinear with the source, and the two micro-lenses are embedded in two distinct host galaxies. We assume that the effect of the host galaxy is constant across the Einstein radius of the microlens. Under this framework, the following terms are introduced into the lensing potential (an extension of the single-plane case discussed in Schneider *et al.* (1992)):

$$\begin{aligned} \psi_{\text{ext}}(x_1, x_2, x_3, x_4) = & \left(\frac{r_1 r_3}{2(r_3 - r_1)} \right) \left[\kappa_1(x_1^2 + x_2^2) + \gamma_{11}(x_1^2 - x_2^2) + 2\gamma_{12}x_1x_2 \right] \\ & + \left(\frac{r_2 r_3}{2(r_3 - r_2)} \right) \left[\kappa_2(x_3^2 + x_4^2) + \gamma_{21}(x_3^2 - x_4^2) + 2\gamma_{22}x_3x_4 \right], \end{aligned} \quad (10)$$

where κ_1 (κ_2) and $(\gamma_{11}(\gamma_{21}), \gamma_{12}(\gamma_{22}))$ correspond to the external convergence and shear parameters of the galaxy in which M_1 (M_2) is embedded. For simplicity, we choose γ_{12} and γ_{22} to be zero, which correspond to

specific orientations of the two galaxies. Note that the various x_i 's in Equation 10 correspond to angular coordinates.

We show the dependence of the amplification factor on the various external convergence/shear parameters in Figure 7. For reference, in each of the panels, we show the isolated microlenses case in black. To ensure that numbers are meaningful with respect to galaxy lenses, we choose $(r_1, r_2, r_3) = (100.0, 200.0, 300.0)$ Mpc. We fix $\theta_3 = 0.00003$ arc-sec and microlens masses are set to $10 M_\odot$ each. For this choice of θ_3 , the curve in black is identical to the red curves from the previous figures.

In the top panel, we consider cases with only external shear (i.e. κ 's are set to zero). When one/both of the two shear parameters is/are non-zero, we note the following: absolute value and phase of the amplification factor oscillate at different rates in comparison to the reference curve in black. In the centre panel, we consider cases with only external convergence. Unlike the previous case with only external shear, we notice a pattern in this case: 'adding' external convergence into the lens system increases the magnitude of absolute values of the amplification factor at low frequencies (~ 10 Hz). In the bottom panel, we examine cases where both external convergence and shear are present in the lens system. One can see that the resultant curves with both non-zero shear and convergence look like combinations of the above panels: the non-zero convergence leads to an increase in the overall magnitude of the oscillations, while the non-zero shear introduces a modification in rate of oscillation.

As mentioned earlier, these observations depict the complex dependence of the amplification factor on the various parameters. Unlike the single lens plane case (especially for the isolated point mass lens), it isn't easy to make predictions on the behaviour of the amplification factor when the values of multiple parameters are varied simultaneously. From our observations, we recommend that the best way to study wave effects in double- (or multi-, in general) plane lensing is to study various possible lens systems case by case, instead of trying to extrapolate results from a set of test cases. Apart from that, we also find that the Monte Carlo integrator provides satisfactory results for the case of $N = 2$. However, for integrals corresponding to higher number of lens planes, one may need to explore alternate methods (e.g., [Feldbrugge, 2020](#)).

5. Conclusions

In this work, we have explored the effects of wave optics in double plane lensing. We have also compared the

wave-optical effects of a double plane lens with a single lens plane consisting of one and two-point mass lenses. We find that only for some arrangements one can identify similar behavior in single and double plane lensing. For example, in some cases, varying the observer position with respect to the source yields a qualitatively similar behavior in both single and double planes. However, apart from this, it is not straightforward to make generalized statements about the behavior of lens systems: the number of parameters is just too large, even for the relatively simple case of two lens planes.

One would expect the complexity to further increase for a large number of lens planes. However, the probability of observing lens system with more than two lens planes is significantly lower. The increase in complexity also holds for double plane lenses if we increase the number of point mass lenses in one or both of the lens planes. The presence of galaxy lenses in such systems would introduce an additional shear and convergence, which is expected to further complicate the analysis. Keeping this in mind, we conclude that the best way to study wave effects in multi-plane lensing is to tackle separate lens systems case by case instead of hoping to make predictions based on a few test cases.

Acknowledgements

RR would like to thank the Department of Science and Technology, Government of India for being awarded the INSPIRE scholarship. AKM would like to thank Council of Scientific and Industrial Research (CSIR) India for financial support through research fellowship No. 524007. Authors acknowledge the use of IISER Mohali HPC facility. Authors would like to thank Kandaswamy Subramanian for valuable comments on the manuscript. This research has made use of NASA's Astrophysics Data System Bibliographic Services.

References

- Abbott, B. P., Abbott, R., Abbott, T. D., *et al.* 2019, Physical Review X, 9, 031040
- Abbott, R., Abbott, T. D., Abraham, S., *et al.* 2020, arXiv e-prints, arXiv:2010.14527
- Asada, H. 2003, Progress of Theoretical Physics, 110, 425
- Baraldo, C., Hosoya, A., & Nakamura, T. T. 1999, Phys. Rev. D, 59, 083001
- Bartelmann, M. 2010, Classical and Quantum Gravity, 27, 233001

Bozza, V., Pietroni, S., & Melchiorre, C. 2020, *Universe*, 6, 106

Broadhurst, T., Diego, J. M., & Smoot, G. F. 2020, arXiv e-prints, arXiv:2006.13219

Broadhurst, T., Diego, J. M., & Smoot, George, I. 2018, arXiv e-prints, arXiv:1802.05273

Broadhurst, T., Diego, J. M., & Smoot, George F., I. 2019, arXiv e-prints, arXiv:1901.03190

Christian, P., Vitale, S., & Loeb, A. 2018, *Phys. Rev. D*, 98, 103022

Diego, J. M., Hannuksela, O. A., Kelly, P. L., *et al.* 2019, *A&A*, 627, A130

Erdl, H., & Schneider, P. 1993, *A&A*, 268, 453

Feldbrugge, J. 2020, arXiv e-prints, arXiv:2010.03089

Kneib, J.-P., & Natarajan, P. 2011, *A&A Rev.*, 19, 47

Kochanek, C. S., & Apostolakis, J. 1988, *MNRAS*, 235, 1073

Lepage, G. P. 2020, arXiv e-prints, arXiv:2009.05112

Li, S.-S., Mao, S., Zhao, Y., & Lu, Y. 2018, *MNRAS*, 476, 2220

Meena, A. K., & Bagla, J. S. 2020, *MNRAS*, 492, 1127

Mishra, A., Meena, A. K., More, A., Bose, S., & Singh Bagla, J. 2021, arXiv e-prints, arXiv:2102.03946

Nakamura, T. T., & Deguchi, S. 1999, *Progress of Theoretical Physics Supplement*, 133, 137

Ohanian, H. C. 1974, *International Journal of Theoretical Physics*, 9, 425

Pejcha, O., & Heyrovský, D. 2009, *ApJ*, 690, 1772

Peters, P. C. 1974, *Phys. Rev. D*, 9, 2207

Schneider, P., Ehlers, J., & Falco, E. E. 1992, *Gravitational Lenses*, doi:10.1007/978-3-662-03758-4

Schneider, P., & Weiss, A. 1986, *A&A*, 164, 237

Smith, G. P., Berry, C., Bianconi, M., *et al.* 2018, *IAU Symposium*, 338, 98

Subramanian, K., & Chitre, S. M. 1984, *ApJ*, 276, 440

Subramanian, K., Rees, M. J., & Chitre, S. M. 1987, *MNRAS*, 224, 283

Takahashi, R., & Nakamura, T. 2003, *ApJ*, 595, 1039

Umetsu, K. 2020, *A&A Rev.*, 28, 7

Witt, H. J., & Petters, A. O. 1993, *Journal of Mathematical Physics*, 34, 4093

Yamamoto, K. 2003, arXiv e-prints, astro

Appendix A. Geometric Optics

For greater insights into Figure 2, we here show the critical lines and caustics corresponding to the various cases discussed earlier. When the source happens to be outside the caustic, three images of the source are formed. However, when the source moves into the caustic, an additional two images are produced, thereby increasing the complexity of the amplification factor.

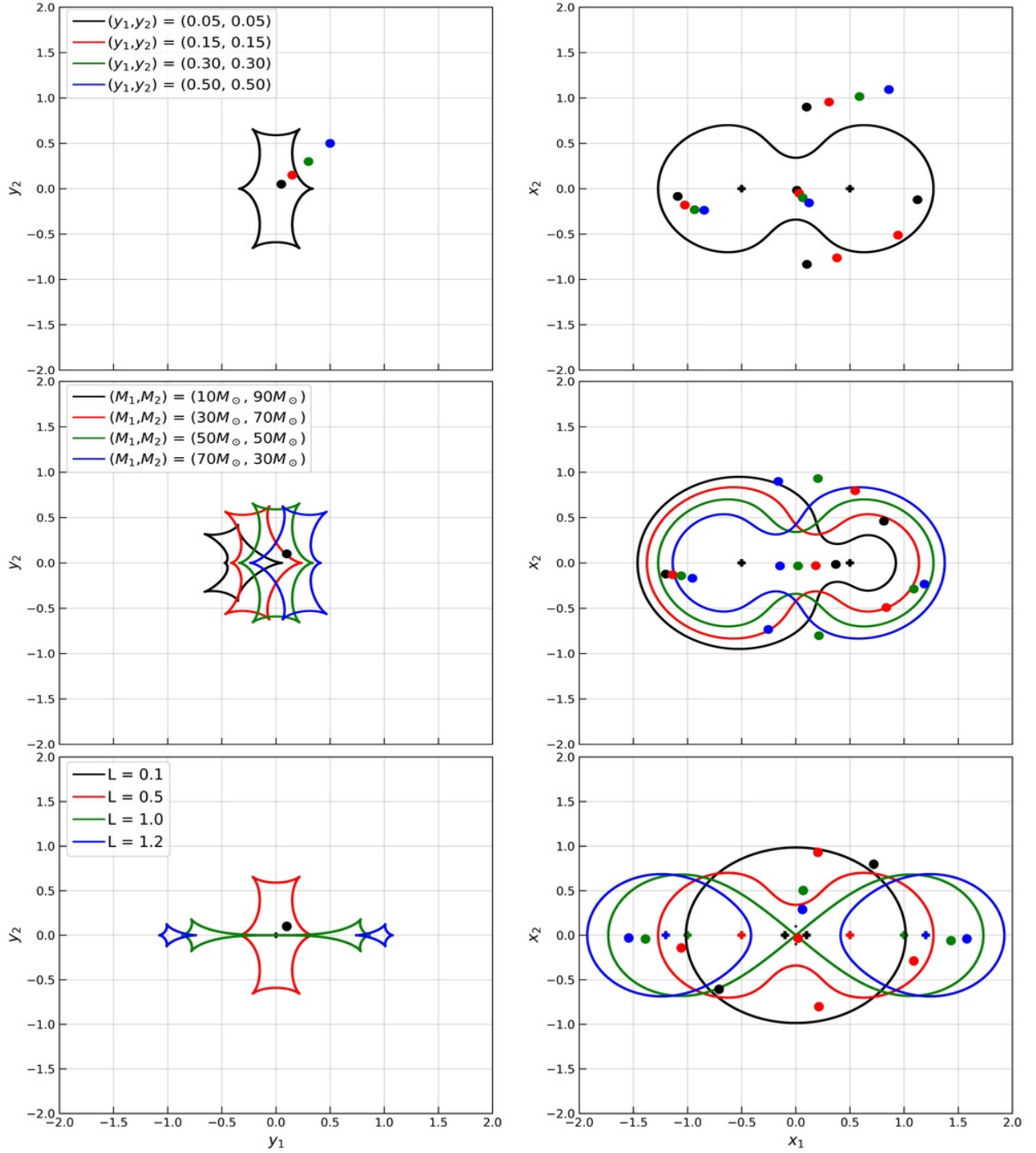


Figure 8. Caustics (left) and Critical lines (right) corresponding to the cases discussed in Figure 2. The various filled circles correspond to the position of the source (images) in the left (right) panel. When the source happens to be outside (inside) the caustic, three (five) images are formed.